HHS Public Access

Author manuscript

Biotechnol Bioeng. Author manuscript; available in PMC 2020 September 01.

Published in final edited form as:

Biotechnol Bioeng. 2019 September ; 116(9): 2377–2392. doi:10.1002/bit.27075.

Micropatterned substrates with physiological stiffness promote cell maturation and Pompe disease phenotype in human induced pluripotent stem cell-derived skeletal myocytes

Nunnapas Jiwlawat[1], **Eileen M. Lynch**[1], **Brett N. Napiwocki**[2,3], **Alana Stempien**[2,3], **Randolph S. Ashton**[2,3,5], **Timothy J Kamp**[4,5,6], **Wendy C. Crone**[2,3,5,7,*], **Masatoshi Suzuki**[1,3,5,*]

[1]Department of Comparative Biosciences, University of Wisconsin, Madison, WI 53706, USA

[2]Wisconsin Institute for Discovery, University of Wisconsin, Madison, WI 53706, USA

[3]Department of Biomedical Engineering, University of Wisconsin, Madison, WI 53706, USA

[4]Department of Medicine, University of Wisconsin, Madison, WI 53706, USA

[5]The Stem Cell and Regenerative Medicine Center, University of Wisconsin, Madison, WI 53706, USA

[6]Department of Cell and Regenerative Biology, University of Wisconsin, Madison, WI 53706, USA

[7]Department of Engineering Physics, University of Wisconsin, Madison, WI 53706, USA

Abstract

Recent advances in bioengineering have enabled cell culture systems that more closely mimic the native cellular environment. Here we demonstrated that human induced pluripotent stem cell (iPSC)-derived myogenic progenitors formed highly-aligned myotubes and contracted when seeded on two-dimensional micropatterned platforms. The differentiated cells showed clear nuclear alignment and formed elongated myotubes dependent on the width of the micropatterned lanes. Topographical cues from micropatterning and physiological substrate stiffness improved the formation of well-aligned and multi-nucleated myotubes similar to myofibers. These aligned myotubes exhibited spontaneous contractions specifically along the long axis of the pattern. Notably, the micropatterned platforms developed bundle-like myotubes using patient-derived iPSCs with a background of Pompe disease (glycogen storage disease type II), and even enhanced the disease phenotype as shown through the specific pathology of abnormal lysosome accumulations. A highly-aligned formation of matured myotubes holds great potential in further understanding the process of human muscle development, as well as advancing *in vitro* pharmacological studies for skeletal muscle diseases.

[*]Correspondence: Masatoshi Suzuki: 2015 Linden Dr., Madison, WI 53706, USA; Tel: 608-262-4264; Fax: 608-890-3667; masatoshi.suzuki@wisc.edu; Wendy C. Crone: 1500 Engineering Drive, Madison, WI 53706, USA; Tel: 608-262-8384; Fax: 608-263-7451; wendy.crone@wisc.edu.

Conflicts of interest: The authors declare no competing interests.

Additional Information

Supplementary information includes three Supplemental Figures, the information about Supplementary Videos, and ten Supplemental Videos which can be found with this article online.

Keywords

Micropattern; human induced pluripotent stem cells; skeletal myocytes; *in vitro* modeling; substrate stiffness; Pompe disease

1. Introduction

Neuromuscular disorders cause impaired muscle function either directly from muscle pathology and/or indirectly from pathology in the central nervous system. Many neuromuscular diseases such as muscular dystrophies are caused by genetic mutations and have limited treatment options. Numerous pre-clinical studies using animal models have identified potential treatments for neuromuscular diseases (Blat & Blat, 2015; Vainzof et al., 2008) but the results have often been unsatisfactory in subsequent clinical trials. New approaches for pre-clinical evaluation of therapeutic approaches using *in vitro* models with human muscle cells could be advantageous when considering the potential for clinical translation.

The advent of human pluripotent stem cells (PSCs), embryonic stem cells (ESCs) and induced pluripotent stem cells (iPSCs), provides an indefinite cell source for cell-based therapies and *in vitro* modeling (Hosoyama, Van Dyke, & Suzuki, 2012; Rinaldi & Perlingeiro, 2014; Roca, Requena, Edel, & Alvarez-Palomo, 2015). Specifically, human skeletal myogenic progenitors can be derived from human PSCs (Tedesco & Cossu, 2012; Zhu et al., 2014) using either exogenous expression of myogenic genes such as *PAX3*, *PAX7*, and *MYOD* (Abujarour et al., 2014; Darabi et al., 2012; Maffioletti et al., 2015; Skoglund et al., 2014; Tanaka et al., 2013) or small molecules and growth factors (Barberi et al., 2007; Borchin, Chen, & Barberi, 2013; Caron et al., 2016; Chal et al., 2016; I. Y. Choi et al., 2016; Hosoyama, McGivern, Van Dyke, Ebert, & Suzuki, 2014; Hwang et al., 2013; Shelton et al., 2014; Xu et al., 2013). Our group recently established a transgene-free protocol using free-floating spherical culture to generate myogenic progenitors from human PSCs (Hosoyama et al., 2014). Importantly, human iPSCs generated from both healthy donors and patients with neuromuscular disorders can be differentiated into myotubes using our culture protocol (Hosoyama et al., 2014). Myotubes derived from patient-specific iPSC lines are a valuable resource for studying neuromuscular disease mechanisms and testing potential drug therapies (Rinaldi & Perlingeiro, 2014; Roca et al., 2015).

Recent innovations in bioengineering provide multi-factorial and multi-dimensional controlled platforms for biomedical research beyond the traditional culture systems that use unpatterned substrates (Maffioletti et al., 2018; Nakamoto, Wang, Kawazoe, & Chen, 2014; Rao, Qian, Khodabukus, Ribar, & Bursac, 2018; Salick et al., 2014; Serena et al., 2016). Among these approaches, two-dimensional (2D) geometry cues significantly influence cell morphology and behavior in culture. 2D micropatterned lanes have shown positive effects on cell alignment during differentiation of various cell types including smooth muscle (Nakamoto et al., 2014), cardiac muscle (Agarwal et al., 2013; Salick et al., 2014), and skeletal muscle (Bettadapur et al., 2016; Duffy, Sun, & Feinberg, 2016; Serena et al., 2016; Zatti et al., 2012). Like adult muscle fibers with linear bundles of myotubes, geometric cues

may further support better alignment, morphology, and maturation in iPSC-derived skeletal myotubes. Moreover, a number of studies have shown that stiffness-controlled substrates influence cell migration, morphology, and phenotypes in differentiating stem cells (Choi, Vincent, Lee, Dobke, & Engler, 2012; Engler, Sen, Sweeney, & Discher, 2006; Hadden et al., 2017; Salick et al., 2014). Using specific stiffness-controlled substrates recapitulating native tissues, for example ~500 Pa - 1 kPa (neuron), ~12 kPa (skeletal muscle), and ~30 kPa (bone), enhanced their differentiation (Discher, Janmey, & Wang, 2005; Engler et al., 2006; Saha et al., 2008). Primary mouse and human myoblasts plated on soft substrates at 12 kPa (Engler et al., 2004) and at 15 kPa (Serena et al., 2010) respectively increased sarcomere formation compared to plating on a rigid substrate. Here we test a hypothesis that the use of micropatterned lanes and physiological substrate stiffness during muscle differentiation improves the alignment and sarcomere formation of human iPSCs-derived myotubes.

Furthermore, we explored the ability of our micropatterned platforms to create *in vitro* models for neuromuscular diseases using patient-derived iPSCs. In this study, we used the iPSC line prepared from fibroblasts of a patient with Pompe disease (glycogen storage disease type II) (Raval et al., 2015). Pompe disease is a lysosomal storage disease caused by mutations of the gene encoding acid alpha-glucosidase (GAA), a lysosomal enzyme essential for converting glycogen into free glucose (Dasouki et al., 2014; Manganelli & Ruggiero, 2013). The muscle pathology demonstrates the accumulation of glycogen in enlarged lysosomes, which causes impaired muscle function in Pompe disease patients (Prater et al., 2013; Thurberg et al., 2006; Werneck, Lorenzoni, Kay, & Scola, 2013).

2. Materials and Methods

2.1 Human iPSC culture

A human iPSC line (IMR90) was received from WiCell (Madison, WI), which was originally generated from fibroblasts of healthy donor by cell reprogramming (J. Yu et al., 2007). A patient-specific iPSC line with a background of Pompe disease (glycogen storage disease type II) was also used in this study. The Pompe disease iPSC line (Raval et al., 2015) was prepared from patient fibroblasts (GM04912, Coriell Institute for Medical Research, Camden, NJ) (J. Yu et al., 2009). All iPSCs were maintained following a feeder-independent protocol (Ludwig et al., 2006). iPSC colonies were plated on a 6-well plate coated with Matrigel (BD Bioscience, San Jose, CA) in mTeSR1 medium, and passaged using Versene (Life Technologies, Carlsbad, CA).

2.2 Skeletal muscle differentiation of human iPSCs

Myogenic progenitors were prepared as described in our previous publications (Hosoyama et al., 2014; Jiwlawat et al., 2017). Human iPSC colonies were lifted using 0.1% collagenase (Life Technologies) to form spherical aggregates (termed EZ spheres). EZ spheres were maintained in the expansion medium [Stemline medium (S-3194, Sigma-Aldrich, St. Louis, MO) supplemented with 100 ng/ml recombinant human FGF2 (WiCell), 100 ng/ml human EGF (EMD Millipore, Burlington, MA), heparin sulfate (Sigma-Aldrich), and penicillin/streptomycin/amphotericin B (PSA, 1%v/v; Life Technologies)]. The spheres were passaged weekly by mechanical chopping using a McIlwain tissue chopper (Mickle Laboratory

Engineering, Surrey, UK). After 6 weeks of culture, EZ sphere cells were dissociated by trypsin (TrypLE, Life Technologies). The dissociated cells were then seeded onto micropatterned or unpatterned (as control) platforms. The surfaces of the culture platforms were pre-coated with Matrigel (83.3 μg/ml; Corning Incorporated, Corning, NY). The plated cells were cultured in terminal differentiation medium [Dulbecco's Modified Eagle's Medium (DMEM, Sigma-Aldrich) containing 2% B27 supplement (Life Technologies) and 1% PSA]. Differentiated myocytes were characterized at the 2, 4, and 6 week timepoints depending on the features being investigated. These time points of differentiation were selected based on our previous publications (Hosoyama et al., 2014; Jiwlawat et al., 2017).

2.3 Micropatterned substrates

Micropatterns on rigid substrates were prepared as described (Salick et al., 2014) and also outlined in Fig. 1, **Left**. Briefly, the micropatterned lanes on the silicon wafer were created by photolithography techniques. To produce a polydimethylsiloxane (PDMS) stamp, a 10:1 mixture of base (Sylgard 184 kit, Dow Corning Corporation, Auburn, MI, USA) to curing agent was poured on the Si wafer and cured overnight at 60°C. The PDMS stamps were used to pattern alkanethiol on Ti/Au-coated glass slides with Young's modulus of 63 GPa (Ashby, Shercliff, & Cebon, 2018). Afterwards, surface-initiated atom transfer radical polymerization (Si-ATRP) was used to graft non-adherent polyethylene glycol (PEG) brushes. Matrigel (Corning Incorporated) was then coated and attached to the highly-adherent gold regions of the slides and not to the PEG regions (Sha, Lippmann, McNulty, Ma, & Ashton, 2013). This rigid substrate was used for the optimization of lane features, shown in Fig. 2 and Fig. 3.

The PDMS substrate with Young's modulus of 15kPa was produced from the mixture of Sylgard 184 and Sylgard 527 (Dow Corning Corporation, Midland, MI) as previously described (Palchesko, Zhang, Sun, & Feinberg, 2012). The substrate stiffness was also confirmed independently with a uniaxial tensile test using an Instron 5548 MicroTester mechanical testing machine with a 10N load cell (data not shown). The PDMS stamp was coated with Matrigel (Corning Incorporated) overnight, and then stamped onto a polyvinyl alcohol (PVA) film (H. Yu, Xiong, Tay, Leong, & Tan, 2012). The PVA film transferred the micropatterned Matrigel-coated lanes onto the PDMS substrate (Fig. 1, **right**). The PVA film was then dissolved with PBS and a non-ionic surfactant, Pluronic F-127 (Sigma-Aldrich), was coated on non-Matrigel lane spaces to block cell adhesion.

2.4 Immunocytochemistry

Immunocytochemistry was performed as described in our recent publication (Jiwlawat et al., 2017). For myosin heavy chain [MHC; clone MF20, 1:40, Developmental Studies Hybridoma Bank (DSHB), Iowa City, IA, USA] or titin (clone 9D10, 1:40, DSHB) staining, cells were fixed with ice-cold methanol for 10 minutes. For laminin (clone L9393, 1:100, Sigma-Aldrich), myogenin (MyoG), and Pax7 staining, cells were fixed in 4% paraformaldehyde (PFA) for 20 minutes. The fixed cells were permeabilized with 0.2% Triton-X 100 for 10 minutes and blocked with 10% normal donkey serum for 1 hour. To identify MyoG or acetylcholine receptor expression on MHC-positive myotubes, anti-MyoG antibody (clone M-225, rabbit polyclonal, 1:400, Santa Cruz Biotechnologies, Dallas, TX)

or alpha-bungarotoxin antibody conjugated with Alexa Fluor 488 (1:200, Molecular Probes, Eugene, OR) was co-labeled with the antibody against MHC. To examine the location of Pax7 and MyoG expression on the micropatterned myotubes, rabbit polyclonal anti-MyoG antibody was co-labeled with mouse monoclonal antibodies against Pax7 (clone Pax7, 1:40, DSHB). After incubating the primary antibody with 0.1% Triton-X 100 in phosphate-buffered saline overnight at 4°C, the cells were stained with secondary antibodies conjugated to Alexa Fluor 488 or Cy3 (anti-IgG, 1:1,000, Jackson Immunotech Research Laboratories, West Grove, PA). To identify the expression of Pax7 and MyoG in myotubes, anti-MHC antibodies directly conjugated with Alexa Fluor 660 were used. Cell nuclei were labeled with Hoechst 33258 nuclear dye (0.5 mg/ml in PBS, Sigma-Aldrich). To identify lysosome vesicles, the cells were fixed in 2% PFA for 30 minutes, permeabilized in digitonin (50 mg/ml in PBS, Sigma-Aldrich) for 10 minutes, blocked with 10% normal goat serum for 1 hour, immunostained with the antibody against Lysosomal-associated membrane protein 1 (LAMP1; clone H4A3, 1:200, DSHB) overnight at 4°C, and incubated with the secondary antibody conjugated to Cy3. LAMP1-labeled cells were then incubated with anti-MHC antibodies directly conjugated with Alexa Fluor 488 (clone MF20, 1:100, eBioscience, San Diego, CA) to identify myotubes. The Leica TCS SP8 confocal microscope (Leica, St. Gallen, Switzerland) was used to capture fluorescence images. We repeated at least two independent experiments to confirm the results of cell counting, fusion, and alignment.

2.5 Detailed analyses of cell fusion and alignment in myotubes

Myocyte fusion was evaluated based on the number of nuclei bound to MHC-positive (MHC $^{+}$) myotubes divided by the total Hoechst-positive nuclei in the microscopic field. MHC and Hoechst staining were used to analyze myotubes that were differentiated on a rigid substrate using two types of geometries; micropatterned (n = 15 fields) and unpatterned (n = 16 fields) at 20x microscopic field.

MHC^{+} myotubes at a fixed length of 250 μm [micropatterned (n = 100 myotubes) vs. unpatterned (n = 116 myotubes)] were used to categorize average diameter of myotubes, the angle alignment of myotubes, and chains of fused nuclei on myotubes compared between micropatterned and unpatterned rigid substrates. We analyzed the angles between each MHC $^{+}$ myotube axis and the direction of the pattern from any lane width size. Due to the non-directional orientation of the unpatterned coverslips, a target point was arbitrarily chosen to act as an axis to determine the angle of the myotubes. The angle-determining axis for micropatterned slides was based off the length of the micropatterned features. The diameter at both ends of each myotube was measured and averaged among myotubes that had a length of 250 μm.

Myotubes differentiated on a micropatterned platform showed more chains of fused nuclei compared to myotubes differentiated on an unpatterned platform. To determine which size of micropatterned lane width yielded myotubes with the largest chains of fused nuclei, we counted the amount of multi-nuclei chains that were fused to the myotubes in the micropatterned lanes of varying widths. We observed that myotubes differentiated in micropatterned platforms of different widths had varied numbers of fused nuclei. We then categorized the chains based of the number of nuclei and counted how many times each size

of the chains occurred, which has been represented as events in the Y-bar of the graph in Fig. 3D.

To investigate how a combination of micropatterning and stiffness influenced sarcomere formation, we used MHC staining and calculated how many striated myotubes were observed among four substrate types: unpatterned rigid (n = 10 fields), micropatterned rigid (n = 10 fields), unpatterned soft (n = 16 fields), and micropatterned soft (n = 16 fields) at 63× microscopic field. We then determined which substrate yielded the most myotube striation.

To determine the effect of stiffness on micropatterned lanes, we analyzed micropatterned myotubes plated on the 15 kPa soft substrate, and calculated the fusion index. Fusion index of myotubes differentiated on unpatterned rigid and soft substrates were compared as a control. 6 fields were used to analyze fusion index for all substrate conditions at 40× microscopic field.

MyoG staining was used to verify whether the cells were differentiated into committed myocytes. The differentiated cells were co-stained with MHC to show the myotubes. The number of MyoG positive nuclei was analyzed in the myotubes differentiated on unpatterned rigid (n = 6 fields) and micropatterned soft (n = 6 fields) substrates at 40× microscopic field.

2.6 Skeletal muscle video capture and analysis

To observe the fusion of myotubes after plating onto the micropatterned subsrate, the Lux2 live cell imaging device was used (CytoSMART, Eindhoven, Netherlands). Time-lapse images were taken every 5 minutes for the first two days after plating, and every 10 minutes for two days starting on day 10 post-plating. The CytoSMART portal created video out of the time-lapse images. Myotube contraction was recorded using a Nikon Eclipse TS 100 inverted microscope with a QImaging camera (QImaging, Surrey, BC, Canada). The movies were recorded as AVI files by Q Capture Pro Software (QImaging). Image J was used to save individual frames as TIF files. The images were then uploaded to Ncorr, an open-source Matlab software (Blaber, Adair, & Antoniou, 2015), to perform digital image correlation (DIC). A reference image was set, and subsequent images were analyzed for pixel displacement from the reference image. The pixel displacements were converted into microns to calculate the displacement of the myotubes over the course of a contraction. The maximum displacements for a field of view were graphed to be more representative of a single contraction.

DIC analysis was also used to detect any changes in contraction dynamics that could be a result of the Pompe disease phenotype. Control iPSC-derived myotubes (n = 10 contractions) or Pompe disease iPSC-derived myotubes (n = 9 contractions) were cultured on the micropatterned soft substrate up to 6 weeks. The maximum displacement from multiple contraction events in the myotubes were averaged and analyzed. The number of contractions per minute were extrapolated from 10 or 20 second video clips (n = 7 videos for control, n = 9 videos for Pompe). The number of contractions was counted in individual fibers. The amount of displacements involving the whole unified bundle of myofibers, which we defined as coordinated contractions, was also analyzed.

2.7 Acid α-glucosidase (GAA) enzymatic activity

GAA enzyme activity in iPSC-derived progenitor cells was determined by the standard protocol that has been commonly used for the definitive diagnosis of Pompe disease patients (Manganelli & Ruggiero, 2013). The protein lysates were prepared from EZ spheres at 6 weeks. The spheres were collected, sonicated by an ultrasonic cell disruptor sonicator (Model XL2000, Microson, Barcelona, Spain), and protein concentration was measured (Bradford reagent, Bio-Rad Laboratories, Hercules, CA, USA). The reaction was set up in a 96 well plate with a black bottom. The 4-methylumbelliferyl-α-D-glucoside (4-MUG; Sigma-Aldrich) artificial substrates were added to protein lysate samples, and then hydrolyzed the α1,4 glucose-glucose bond of glycogen to release glucose. The fluorophore 4-methylumbelliferone (4-MU) was the fluorescent product of the hydrolysis reaction. The fluorescence signals were detected by the GloMax®-Multi microplate multimode reader (Promega Corp., Madison, WI). GAA activity in the protein lysates was measured under the reaction at acidic pH 4.3 as previously described (Reuser, Koster, Hoogeveen, & Galjaard, 1978). The value of neutral α-glucosidase activity at neutral pH 6.7 was also evaluated as a control (Reuser et al., 1978).

2.8 Electron microscopy

The cells were fixed in 2% PFA and 2.5% glutaraldehyde in 0.1 M cacodylate buffer for 1 hour, and stored in 0.1 M cacodylate buffer overnight at 4°C. The fixed cells were incubated in 1% osmium tetroxide for 1 hour, dehydrated through ethanol gradient, and embedded in Durcapan (Sigma-Aldrich). After polymerization, the cells were sectioned at 60 nm, and stained with lead citrate and uranium acetate. Electron microscopic images were captured by a Philips CM120 transmission electron microscope (Philips, Eimdhoven, The Netherlands).

2.9 Statistical Analysis

The GraphPad Prism software (La Jolla, CA) was used for statistical analysis. The data was presented as mean ± SEM. Unpaired two-tailed Student's *t*-test was performed to compare two groups. One-way ANOVA with Tukey post hoc test was calculated to compare multiple groups. In Fig. 5, differences in fusion index and % striated myotubes were calculated using two-way ANOVA with terms in the model for patterning (unpattern vs. micropatterned) and surface stiffness (rigid vs. soft), and their interaction. We used the Tukey method to adjust for the multiple comparisons. Differences were considered significant when $p<0.05$.

3 Results

3.1 Micropatterned lanes enhance linear alignment, nuclei fusion, and diameter of iPSC-derived myotubes compared to an unpatterned platform

Micropatterns on rigid substrates were prepared as described (Salick et al., 2014; Sha et al., 2013) (Fig. 1). The micropatterned rigid substrate was initially used to optimize and characterize plating conditions using a healthy control iPSC line (IMR90) (Fig. 2 and Fig. 3). Human myogenic progenitors were prepared from human iPSCs using our sphere-based culture method (Hosoyama et al., 2014) and then seeded on rigid substrates with two-dimensional micropatterned lanes (15 - 100 μm). As a preliminary observation, we

optimized the cell density of myogenic progenitors for plating on the micropatterned substrates (data not shown). Plating the cells with low density (less than 100,000 cells per cm^2) reduced myotube formation; on the other hand, exceeding a cell density of 200,000 cells per cm^2 showed poor distribution of plated cells with excessive debris accumulation and cell clumping. Although we used 150,000 cells per cm^2 in this study, additional optimizations of cell density may be required when using different iPSC lines.

We analyzed the level of myotube formation after 2 weeks of differentiation, because our previous studies demonstrated that myogenic progenitors could form myotubes after 2 weeks of terminal differentiation when plated on coverslips (Hosoyama et al., 2014; Jiwlawat et al., 2017). At this timepoint, elongated myotubes were identified on both unpatterned and micropatterned glass substrates (Fig. 2A). The cells on unpatterned substrates were less organized in regards to cell alignment and were also branched more (Fig. 2A, **left**). In contrast, the myotubes on micropatterned substrates were highly aligned and followed the longitudinal direction of the patterns (Fig. 2A, **right**). We next analyzed the angle alignment of each myotube and counted the number of myotubes with specific angle alignment (Fig. 2B). When cultured on micropatterned lanes, the myotubes were distributed within 15° from the orientation of the patterned lanes, which act as an axis. The unpatterned myotubes had no preferential direction and were distributed between 15° and 165° (Fig. 2B). The fusion index was also analyzed by counting the number of Hoechst-positive nuclei fused on MHC^+ myotubes and divided by total Hoechst number. The fusion index was significantly higher in micropatterned myotubes (31.9 ± 1%; n = 15 fields) compared to myotubes on an unpatterned platform (16.5 ± 1%; n = 16 fields; $p < 0.01$) (Fig. 2C). Furthermore, the micropatterned substrate significantly increased the diameter of MHC^+ myotubes (6.5 ± 0.1 μm in micropatterned vs. 4.3 ± 0.1 μm in unpatterned; $p < 0.01$) (Fig. 2D).

3.2 The width of micropatterned spaces influenced nuclear alignment in myotubes

We next asked how patterned lane width influenced cell alignment and fusion of the myotubes. Myogenic progenitors were seeded onto glass substrates with various micropatterned lane widths (15-105 μm) (Fig. 3A). In the narrowest lanes of 15 or 25 μm width, only a small number of myotubes could be identified, and most myotubes were detached several weeks later (Fig. 3B). In contrast, the myotubes in the 105 μm lane had small branches and less alignment, similar to the unpatterned culture (Fig. 3B). Next, we determined how mononucleated myoblasts fused to form multinucleated myotubes within a fixed window length (Fig. 3C and D). By counting the occurrence of aligned cell nuclei in fused myotubes, we expected to find a specific range of lane widths that significantly enhanced myotube fusion (Salick et al., 2014). In the unpatterned culture or patterned lanes with 55 μm width or smaller, the majority of myotubes (~83%) had a single nucleus (i.e. did not form nuclear chains) (Fig. 3D). However, in wider lanes (85 - 105 μm) the percentage of myotubes with a single nucleus was less (46 - 58%). Specifically in the lanes at 85 μm width, there were more myotubes with chains of two, three, and four nuclei together (28%, 14%, and 9% per total occurrences), compared to the unpatterned culture (14%, 2%, and 0%) (Fig. 3D). Notably, this lane width was approximated as the diameter of a muscle fiber

in vivo (Sale, 2014). As 85 μm lanes yielded more multinucleated myotubes on the micropatterned platform, this width was used in the subsequent investigations.

3.3 A micropatterned soft substrate promotes a functionally mature phenotype in iPSC-derived myotubes

Having first determined the effects of micropatterning on skeletal myocyte differentiation using a rigid substrate, we next tested the hypothesis that micropatterned topographical cues and substrate stiffness could both improve muscle differentiation and maturation of the plated progenitor cells. We prepared micropatterned substrates with physiologically relevant stiffness (~15 kPa Young's modulus). Using an alternative patterning method, micropatterned lanes of Matrigel were transferred to the soft polydimethylsiloxane (PDMS) substrate and progenitors were then seeded on the Matrigel-coated lanes (Fig. 1, **right**).

The micropatterned culture platform with physiological stiffness (*i.e.* micropatterned soft) was compared to the unpatterned rigid substrate. At 1 week of differentiation, randomly-oriented myotubes with fusion of a few nuclei were identified on the unpatterned rigid substrate (Fig. 4A and C). In contrast, the micropatterned substrate with physiological stiffness promoted multi-nuclear fusion in MHC^+ myotubes (Fig. 4B and D). At 4 weeks in culture, the myotubes still maintained their alignment and bundle-like morphology in the micropatterned lanes with controlled stiffness (Fig. 4F). Using immunocytochemistry for MHC, we identified striated patterns in the differentiated myotubes which represent sarcomeric organization (Fig. 4G and H). At the same timing of differentiation, obvious sarcomere organization was not yet visible in the myotubes on the unpatterned rigid surface (Fig. 4G). However, clear striations were already formed in the myotubes cultured in micropatterned lanes with physiological stiffness (Fig. 4H). Myotube striations were then identified on unpatterned rigid substrates at 6 weeks of differentiation, as seen in the myotubes on micropatterned soft substrates (Supplementary Figure 1).

We determined whether spontaneous contractions could be observed in the myotubes plated on the micropatterned lanes with physiological stiffness. The differentiated myotubes were regularly monitored under light microscopy, and the contractions were recorded using a CCD camera. In the myotubes on both micropatterned and unpatterned substrates, the spontaneous contraction was first observed at 4 weeks of differentiation. The myotubes on unpatterned features were randomly distributed and less-coordinated (Supplementary Video S1A); whereas, the micropatterned myotubes were highly-aligned and well-coordinated with active contractions like bundled fibers (Supplementary Video S1B). The spontaneous contractions persisted at 6 weeks of differentiation on both unpatterned substrates (Supplementary Video S1C) and micropatterned lanes (Supplementary Videos S1D and S1E). Using these videos, we performed digital image correlation (DIC) analysis and generated displacement data in the x and y directions (longitudinal or perpendicular to the lane) over the period of a single contraction (Fig. 4I, J, and K). The maximum displacements from the entire field of view is shown for three separate contraction events (Fig. 4J), and displacement values from specific locations are plotted over the duration of a single contraction event (Fig. 4K). The unpatterned myotubes had similar and minimal displacements in both directions, while the myotubes plated on micropatterned lanes had a

much stronger peak in the longitudinal axis with minimal displacement in the perpendicular direction (Fig. 4K). These results indicate that more robust and aligned contractions could be detected in micropatterned myotubes compared to unpatterned ones.

We also applied live-cell imaging to observe the fusion of myotubes after plating onto the micropatterned substrate. Time-lapse video shows migration of individual cells and their dynamic fusion and elongation to form myotubes (Supplementary Videos S2A-2D). Additionally, we monitored clustering of post-synaptic acetylcholine receptors (AChRs) in the micropatterned myotubes. Post-synaptic organization of acetylcholine receptors is necessary for proper formation of a neuromuscular junction. AChR was positively located at the edge of MHC^+ myotubes (Fig. 4L).

To further confirm the effect of substrate stiffness on sarcomere formation, four different culture conditions were tested with modified topographical cues and physiological substrate stiffness: unpatterned rigid, micropatterned rigid, unpatterned soft, and micropatterned soft substrates. We collected differentiated myotubes at 2 weeks of differentiation and stained for MHC. The fusion index was higher in micropatterned myotubes (34.3 ± 4%; n = 6 fields) compared to myotubes on an unpatterned platform (24.2 ± 3%; n = 6 fields) (Fig. 5A, B, and E). Soft substrate increased fusion index in the myotubes (unpatterned soft, 32.5 ± 5%; n = 6 fields; micropatterned soft, 42.8 ± 4%; n = 6 fields; Fig. 5B, D, and E). We calculated differences in fusion index using two-way ANOVA with terms in the model for patterning, stiffness and their interaction. Although patterning did not reach statistical significance ($P=0.06$), a significant difference was observed in stiffness ($P<0.05$). The interaction between patterning and stiffness did not reach statistical significance.

In our recent study, the striations were less apparent at 2 weeks when myotubes were plated on coverslips (*i.e.* a unpatterned rigid surface), but sarcomere patterns became more obvious following a long-term differentiation up to 12 weeks (Jiwlawat et al., 2017). Consistent with our previous results, obvious sarcomere structures were not characterized in the myotubes when plated on unpatterned rigid substrates at 2 weeks of differentiation (Fig. 5A). Similarly, the myotubes on micropatterned rigid substrates did not show sarcomere patterns (Fig. 5B). Regardless of topographic cues, soft substrates promoted sarcomere formation in the myotubes (Fig. 5C and D). When we quantified the percentage of striated myotubes, a higher percentage of striated myotubes was identified on soft substrates (unpatterned soft 42.65 ± 4%; n = 16 fields) compared to on unpatterned rigid substrate (0.62 ± 0%; n = 10 fields; $P<0.01$) or micropatterned rigid substrate (3.81 ± 1%; n = 10 fields; $P<0.01$) (Fig. 5F). Notably, micropatterning further promoted sarcomare formation when myotubes are plated on the micropatterned soft platform (58.79 ± 4%; n = 16 fields; $P<0.05$ vs. unpatterned soft) (Fig. 5F). The analysis using two-way ANOVA revealed that a significant difference was observed in patterning ($P<0.01$), stiffness ($P<0.05$), and the interaction between patterning and stiffness ($P<0.05$). The sarcomere length from Z band to Z band was unchanged between two micropatterned conditions (micropatterned rigid, 2.49 ± 0.2 μm; micropatterned soft, 2.50 ± 0.2 μm; n=10 myotubes for each group).

3.4 Differentiation of patient iPSC-derived myotubes on micropatterned culture platforms

In order to test ability of this culture system to be used for *in vitro* disease modeling purposes, we next prepared myogenic progenitors from the iPSC line derived from Pompe disease patients (Supplementary Figure 2). We confirmed that the progenitors derived from Pompe disease-iPSCs formed MHC^+ myotubes on unpatterned rigid and micropatterned soft substrates (Fig. 6). MHC^+ myotubes were similarly observed in the myotubes prepared from control iPSCs. Further, we identified titin+ myotubes in Pompe iPSC-derived myotubes, with lengths over 750 μm which was similar to that of the lengths of control iPSC-derived myotubes at 2 weeks of differentiation (Fig. 6A). Most of the nuclei in the MHC^+ myotubes were positive for myogenin (MyoG), a marker of committed myoblasts (Jiwlawat et al., 2017; Madden, Juhas, Kraus, Truskey, & Bursac, 2015) (Fig. 6B). On the unpatterned rigid substrate, myotubes showed random orientation with only a few nuclear fusion events (Fig. 6B, **left**). In contrast, micropatterned lanes with controlled stiffness enhanced formation of multinucleated myotubes in both Pompe disease and control cell lines (Fig. 6B, **right**). Myogenin expression also seemed to be increased as a result of micropatterning, as the number of MyoG+ myonuclei was increased on micropatterned lanes (44.95 ± 5% in Pompe vs. 48.99 ± 3% in control; n = 6 fields) compared to unpatterned culture (34.91 ± 2% in Pompe vs. 36.11 ± 4% in control; n = 6 fields) (Fig. 6C). The fusion index appears to be influenced by both micropatterning and substrate stiffness. Similarly as observed in the results above, the fusion index was significantly higher in both Pompe and control-derived myotubes plated on micropatterned soft substrate (Pompe 41.24 ± 5%, control 42.78 ± 4%; n = 6 fields) than on unpatterned rigid substrates (Pompe 24.51 ± 1%, control 24.18 ± 3%; n = 6 fields; $p< 0.05$) (Fig. 6D). Together, the number of MyoG+ myonuclei and the fusion index appeared to be influenced by micropatterning and substrate stiffness.

Patient iPSC-derived myotubes were expected to exhibit specific pathology associated with the disease. We confirmed that Pompe iPSC-derived myogenic progenitors showed a significant reduction of GAA enzyme activity close to zero (0.19 ± 0.06 nmol/hr/mg protein; n=3), while the control iPSC-derived myogenic progenitors maintained a significant level of GAA enzyme activity (55.91 ± 5.02 nmol/hr/mg protein; n=3) (Fig. 7A). On the other hand, the activity of the control enzyme (neutral α-glucosidase) remained normal in both Pompe (70.24 ± 1.74 nmol/hr/mg protein; n=3) and control cells (53.04 ± 2.42 nmol/hr/mg protein; n=3) (Fig. 7A). Interestingly, the level of neutral α-glucosidase was significantly higher in the Pompe iPSC-derived cells compared to the control cells ($P<0.05$). We also analyzed the ultrastructure of iPSC-derived myotubes by electron microscopy (Fig. 7B). Electron microscopy has commonly been used to characterize glycogen accumulation in the muscle biopsies from Pompe disease patients (Thurberg et al., 2006). Pompe iPSC-derived myotubes sustained enlarged lysosomes of multiple sizes, and these lysosomes interrupted sarcomere substructures. The enlarged lysosomes contained various sizes of glycogen granules (right bottom, Fig. 7B). In contrast, control iPSC-derived myotubes maintained intact skeletal myotubes with well-organized striations. This disruption of sarcomere structure by glycogen accumulation and subsequent loss of contractile activity has been documented in Pompe patient muscle biopsy samples (Griffin, 1984; Lim, Li, & Raben, 2014; Thurberg et al., 2006).

Pompe iPSC-derived myotubes were plated on the micropatterned platforms, and immunocytochemistry for lysosomal-associated membrane protein 1 (LAMP1) was performed to identify abnormal enlarged lysosomes in myotubes (Lim et al., 2014; Takikita, Myerowitz, Zaal, Raben, & Plotz, 2009) (Fig. 7D–H). LAMP1-positive signals were widely distributed in the myotubes prepared from Pompe iPSCs on both unpatterned (Fig. 7F) and micropatterned substrates (Fig. 7G and H). Unpatterned and micropatterned myotubes from control iPSCs also contained LAMP1-positive signals, but these signals were weak and scattered (Fig. 7D and E). When analyzing the percentage of the LAMP-positive area per myotube, Pompe iPSC-derived myotubes commonly exhibited more LAMP-postive signals in both unpatterned (0.89 ± 0.4% control, n=10; 5.30 ± 1.3% Pompe; n=11) and micropatterned platforms (1.54 ± 0.5 % control, n=9; 18.9 ± 3.9% Pompe; n=8) (Fig. 7C). Pompe iPSC-derived myotubes plated on micropatterned platforms showed more LAMP-postive signals compared to the unpatterned myotubes ($P<0.05$), suggesting that micropatterned substrates with physiological stiffness highlighted lysosomal abnormality in Pompe iPSC-derived myotubes.

Finally, we analyzed the contraction dynamics of Pompe iPSC-derived myotubes plated on a micropatterned soft substrate using DIC analysis as in Fig. 4. In comparison to the control line, the Pompe myotubes had a significantly reduced level of displacement per contraction (5.4 ± 0.6 μm control, n=10 contractions; 3.3 ± 0.6 μm Pompe, n=9 contractions; $P<0.05$) (Fig. 7I) and less total contractions per minute (384.0 ± 84.5 contractions/minute in control, n=7 videos; 19.7 ± 5.5 contractions/minute in Pompe, n=9 videos; $P<0.01$) (Fig. 7J). The amount of coordinated contractions, which involved whole unified bundle of myofibers, tended to be lower in Pompe iPSC-derived myotubes compared to control cells (10.29 ± 7.7 contractions/minute in control, n=7 videos; 1.3 ± 0.7 contractions/minute in Pompe, n=9 videos), although the difference was not statistically significant (Fig. 7K). While these results are still preliminary with limited number of iPSC lines, our data suggests that Pompe iPSC-derived myotubes plated on a micropatterned substrate can serve as an *in vitro* disease model that exhibits functional deficits.

4. Discussion

Here we demonstrated that human iPSC-derived myogenic progenitors formed highly-aligned myotubes and contracted when seeded on micropatterned platforms. The benefits of micropatterned lanes have been highlighted in previous studies to differentiate human progenitor/stem cells into osteogenic cells (Wang, Song, Kawazoe, & Chen, 2013), adipogenic cells (Y. J. Choi et al., 2016), vascular smooth muscle cells (Kusuma, Smith, Facklam, & Gerecht, 2017; Nakamoto et al., 2014), and cardiac muscle cells (Agarwal et al., 2013; Salick et al., 2014). A micropatterned culture platform was also applied to co-culture with human primary myoblasts from Duchenne muscular dystrophy patients and mesoangioblasts, mesenchymal-like adult progenitor cells associated with the walls of the large blood vessels (Serena et al., 2016). A recent study showed that a micropatterned substrate composed of adhesion-permissive strips could support myofiber formation in human iPSC-derived myogenic cells; although, the study did not fully evaluate various culture conditions such as lane widths, stiffness effects, or micropatterned myofiber contraction (Chal et al., 2016). The confined boundaries of micropatterned lanes may

enhance the community effect on skeletal muscle differentiation (Buckingham, 2003; Gurdon, Tiller, Roberts, & Kato, 1993; Yanagisawa, Mukai, Shiomi, Song, & Hashimoto, 2011), resulting in an increased number of $MyoG^+$ nuclei compared to nuclei in unpatterned geometry. Additionally, we identified AChR expression in human iPSC-derived myotubes, which have been similarly seen in the myotubes seeded on unpatterned coverslips in previous studies (Jiwlawat et al., 2017).

In addition to the effect on cell alignment, micropatterning also enhanced the fusion of neighboring myocytes and myotubes. Increased myotube fusion further promoted the formation of multinucleated myotubes and sarcomere organization. Fusion into nascent myotubes is a common step in differentiation of skeletal muscles, and the level of myotube fusion has been used to assess the progression of myotube differentiation (Tanaka et al., 2013; Yaffe & Feldman, 1965). We tested multiple lane widths and found that myotube formation and maturation was enhanced when using a specific lane width (optimal multinucleation was observed at a lane width of 85 μm). Further, micropatterned myotubes show robust contractions as a bundle along the long axis of the pattern. The cellular architecture in our micropatterned bundle-like structures were quite similar to the “myobundle” in three-dimensional muscle constructs (Madden et al., 2015). Their myobundles were prepared from human primary myogenic progenitors, and showed spontaneous contractions like our 2D micropatterned culture (Madden et al., 2015).

It has been suggested that substrate stiffness impacts differentiation and maturation of skeletal myocytes (particularly elongation, alignment, and striation in myotubes) (Engler et al., 2004). In this study, a 15 kPa soft substrate recapitulating *in vivo* stiffness promoted sarcomere formation in human iPSC-derived myotubes. Our PDMS soft substrate results were consistent with a previous observation that used human primary myoblasts; a soft substrate polyacrylamide (PA) at 15 kPa increased sarcomere formation (Serena et al., 2010). Another study showed that PA substrate stiffness at ~12 kPa accelerated MHC^+ myotube striation in mouse C2C12 cells as early as 2 weeks, although no striation was characterized in the MHC^+ myotubes even after 4 weeks in their culture (Engler et al., 2004). Additionally, we confirmed that more bundle-like contractions were observed on soft substrate but not on rigid substrate when using micropatterned lanes. Soft substrate enhanced the formation of the sarcomere structure, which is the functional unit of muscle contraction (Alter, 2004), and may affect the contraction of myotubes on micropatterned lanes. The viscoelastic property of PDMS may affect the cell-contact dependent motion, which enhanced the uniform cell movement (Murrell, Kamm, & Matsudaira, 2011).

Lastly, the micropatterned substrates with controlled stiffness supported derivation of highly-aligned and multi-nucleated myotubes from patient-derived iPSCs with Pompe disease. Abnormal accumulation of LAMP1-positive lysosomes was identified in Pompe iPSC-derived myotubes which represents one of the pathological features commonly seen in the skeletal muscle tissues of Pompe disease patients (Thurberg et al., 2006), murine models of Pompe disease (GAA knock-out mice) (Lim et al., 2014; Takikita et al., 2009), and patient iPSC-derived myocytes (van der Wal et al., 2017; Yoshida et al., 2017). Similary as previously demostrated in those studies, we could simulate distinct pathological phenotypes of Pompe disease in differentiated myotubes using our micropatterned culture platforms,

including reduced contraction displacement and number of contractions. Micropatterned myotubes derived from patient-specific iPSC lines would be a valuable resource for studying disease mechanisms and testing potential drug therapies in neuromuscular diseases, not limited just to Pompe disease.

Recent works (including ours) have introduced new approaches and benefits to using three-dimensional (3D) culture models of skeletal muscle which result in more structurally and functionally mature myocytes (Jiwlawat et al., 2017; Madden et al., 2015; Maffioletti et al., 2018; Rao et al., 2018). These 3D muscle constructs can be used to model muscular dystrophy (Maffioletti et al., 2018), respond to drug treatment (Madden et al., 2015) and even maintain functionality after being transplanted into mice (Rao et al., 2018). However, 2D micropattern platforms bring different advantages for *in vitro* skeletal muscle modeling. For instance, 2D cell culture allows for much easier analysis of the morphology and behavior of individual muscle cells during live imaging. 2D micropatterned culture platforms require fewer cells compared to 3D cultures, which is another potential advantage when considering large-scale drug screening *in vitro*. As a potential compromise between 2D micropatterned cultures and 3D cultures, one possibility is micromolded gelatin hydrogels which have been shown to promote the long term survival of aligned mouse C2C12 myocytes (Bettadapur et al., 2016). While the PDMS substrate used in the our study can present some challenges for imaging, it is overall of benefit for producing mature skeletal myocytes. Further studies using both 2D and 3D *in vitro* systems would help us to understand different facets of neuromuscular disease mechanisms and to test potential drug therapies.

In conclusion, human iPSC-derived myogenic progenitors were cultured on two-dimensional micropatterned platforms and a significant improvement in cell alignment, myotube fusion, and sarcomere formation was observed in specific feature geometries. The myotubes in micropatterned lanes were well-aligned and formed a bundle, which resembles myofibers. Myotubes differentiated on a micropatterned platform had increased nuclear fusion, more myogenin-positive nuclei, and larger fiber diameters compared to unpatterned substrates. Substrates with a physiological stiffness increased the rate of maturation by promoting earlier organization of sarcomere structures. To acheive better *in vitro* modeling for studying myogenesis and muscle pathology, additional optimizations of culture conditions would help to determine how we can further improve mytube differentiation and maturation compared to other extisting approaches and how long the micropatterned myotubes can be maintained in culture. Formation of highly-aligned myofiber-like structures in the soft substrate micropatterned platform holds great potential in further understanding the process of myofilament formation and maturation in human myogenic progenitors, as well as advancing *in vitro* pharmacological studies for neuromuscular diseases.

Supplementary Material

Refer to Web version on PubMed Central for supplementary material.

Acknowledgments

The antibodies for Pax7, myogenin (F5D), titin (9D10), and myosin heavy chain (MF20) were obtained from the DSHB developed under the NICHD and maintained by the University of Iowa.

Grant Information:

The first author (N.J.) would like to thank the financial support from the Royal Thai Government Scholarship. This work was supported by grants from the ALS Association (15-IIP-201, M.S.), NIH/NINDS (R01NS091540, M.S.), the University of Wisconsin Stem Cell and Regenerative Medicine Center (M.S. and E.M.L.), and the University of Wisconsin Foundation (M.S). B.N.N., A.S. and W.C.C. were supported by the Karen Thompson Medhi Professorship, Graduate School, and Office of the Vice Chancellor for Research and Graduate Education at the University of Wisconsin-Madison.

References

Abujarour R, Bennett M, Valamehr B, Lee TT, Robinson M, Robbins D, … Flynn P. (2014). Myogenic differentiation of muscular dystrophy-specific induced pluripotent stem cells for use in drug discovery. Stem Cells Transl Med, 3(2), 149–160. doi:10.5966/sctm.2013-0095 [PubMed: 24396035]

Agarwal A, Farouz Y, Nesmith AP, Deravi LF, McCain ML, & Parker KK (2013). Micropatterning Alginate Substrates for. Adv Funct Mater, 23(30), 3738–3746. doi:10.1002/adfm.201203319 [PubMed: 26213529]

Alter JM (2004). Science of Flexibility. In (third ed., pp. 19–25). Illinois: Human Kinetics.

Ashby MF, Shercliff HS, & Cebon D (2018). Materials: engineering, science, processing and design: Butterworth-Heinemann.

Barberi T, Bradbury M, Dincer Z, Panagiotakos G, Socci ND, & Studer L (2007). Derivation of engraftable skeletal myoblasts from human embryonic stem cells. Nat Med, 13(5), 642–648. doi: 10.1038/nm1533 [PubMed: 17417652]

Bettadapur A, Suh GC, Geisse NA, Wang ER, Hua C, Huber HA, … McCain ML. (2016). Prolonged Culture of Aligned Skeletal Myotubes on Micromolded Gelatin Hydrogels. Sci Rep, 6, 28855. doi: 10.1038/srep28855 [PubMed: 27350122]

Blaber J, Adair B, & Antoniou A (2015). Ncorr: Open-Source 2D Digital Image Correlation Matlab Software. Experimental Mechanics, 55(6), 1105–1122. doi:10.1007/s11340-015-0009-1

Blat Y, & Blat S (2015). Drug Discovery of Therapies for Duchenne Muscular Dystrophy. J Biomol Screen, 20(10), 1189–1203. doi:10.1177/1087057115586535 [PubMed: 25975656]

Borchin B, Chen J, & Barberi T (2013). Derivation and FACS-Mediated Purification of PAX3+/PAX7+ Skeletal Muscle Precursors from Human Pluripotent Stem Cells. Stem Cell Reports, 1(6), 620–631. doi:10.1016/j.stemcr.2013.10.007 [PubMed: 24371814]

Buckingham M (2003). How the community effect orchestrates muscle differentiation. Bioessays, 25(1), 13–16. doi:10.1002/bies.10221 [PubMed: 12508277]

Caron L, Kher D, Lee KL, McKernan R, Dumevska B, Hidalgo A, … Schmidt U. (2016). A Human Pluripotent Stem Cell Model of Facioscapulohumeral Muscular Dystrophy-Affected Skeletal Muscles. Stem Cells Transl Med, 5(9), 1145–1161. doi:10.5966/sctm.2015-0224 [PubMed: 27217344]

Chal J, Al Tanoury Z, Hestin M, Gobert B, Aivio S, Hick A, … Pourquie O. (2016). Generation of human muscle fibers and satellite-like cells from human pluripotent stem cells in vitro. Nat Protoc, 11(10), 1833–1850. doi:10.1038/nprot.2016.110 [PubMed: 27583644]

Choi IY, Lim H, Estrellas K, Mula J, Cohen TV, Zhang Y, … Lee G. (2016). Concordant but Varied Phenotypes among Duchenne Muscular Dystrophy Patient-Specific Myoblasts Derived using a Human iPSC-Based Model. Cell Rep, 15(10), 2301–2312. doi:10.1016/j.celrep.2016.05.016 [PubMed: 27239027]

Choi YJ, Kim TG, Jeong J, Yi HG, Park JW, Hwang W, & Cho DW (2016). 3D Cell Printing of Functional Skeletal Muscle Constructs Using Skeletal Muscle-Derived Bioink. Adv Healthc Mater, 5(20), 2636–2645. doi:10.1002/adhm.201600483 [PubMed: 27529631]

Choi YS, Vincent LG, Lee AR, Dobke MK, & Engler AJ (2012). Mechanical derivation of functional myotubes from adipose-derived stem cells. Biomaterials, 33(8), 2482–2491. doi:10.1016/j.biomaterials.2011.12.004 [PubMed: 22197570]

Darabi R, Arpke RW, Irion S, Dimos JT, Grskovic M, Kyba M, & Perlingeiro RC (2012). Human ES- and iPS-derived myogenic progenitors restore DYSTROPHIN and improve contractility upon transplantation in dystrophic mice. Cell Stem Cell, 10(5), 610–619. doi:10.1016/j.stem.2012.02.015 [PubMed: 22560081]

Dasouki M, Jawdat O, Almadhoun O, Pasnoor M, McVey AL, Abuzinadah A, … Dimachkie MM. (2014). Pompe disease: literature review and case series. Neurol Clin, 32(3), 751–776, ix. doi:10.1016/j.ncl.2014.04.010 [PubMed: 25037089]

Discher DE, Janmey P, & Wang YL (2005). Tissue cells feel and respond to the stiffness of their substrate. Science, 310(5751), 1139–1143. doi:10.1126/science.1116995 [PubMed: 16293750]

Duffy RM, Sun Y, & Feinberg AW (2016). Understanding the Role of ECM Protein Composition and Geometric Micropatterning for Engineering Human Skeletal Muscle. Ann Biomed Eng, 44(6), 2076–2089. doi:10.1007/s10439-016-1592-8 [PubMed: 26983843]

Engler AJ, Griffin MA, Sen S, Bonnemann CG, Sweeney HL, & Discher DE (2004). Myotubes differentiate optimally on substrates with tissue-like stiffness: pathological implications for soft or stiff microenvironments. J Cell Biol, 166(6), 877–887. doi:10.1083/jcb.200405004 [PubMed: 15364962]

Engler AJ, Sen S, Sweeney HL, & Discher DE (2006). Matrix elasticity directs stem cell lineage specification. Cell, 126(4), 677–689. doi:10.1016/j.cell.2006.06.044 [PubMed: 16923388]

Griffin JL (1984). Infantile acid maltase deficiency. II. Muscle fiber hypertrophy and the ultrastructure of end-stage fibers. Virchows Arch B Cell Pathol Incl Mol Pathol, 45(1), 37–50. [PubMed: 6199886]

Gurdon JB, Tiller E, Roberts J, & Kato K (1993). A community effect in muscle development. Curr Biol, 3(1), 1–11. [PubMed: 15335872]

Hadden WJ, Young JL, Holle AW, McFetridge ML, Kim DY, Wijesinghe P, … Choi YS. (2017). Stem cell migration and mechanotransduction on linear stiffness gradient hydrogels. Proc Natl Acad Sci U S A, 114(22), 5647–5652. doi:10.1073/pnas.1618239114 [PubMed: 28507138]

Hosoyama T, McGivern JV, Van Dyke JM, Ebert AD, & Suzuki M (2014). Derivation of myogenic progenitors directly from human pluripotent stem cells using a sphere-based culture. Stem Cells Transl Med, 3(5), 564–574. doi:10.5966/sctm.2013-0143 [PubMed: 24657962]

Hosoyama T, Van Dyke J, & Suzuki M (2012). Applications of skeletal muscle progenitor cells for neuromuscular diseases. Am J Stem Cells, 1(3), 253–263. [PubMed: 23671812]

Hwang Y, Suk S, Lin S, Tierney M, Du B, Seo T, … Varghese S. (2013). Directed in vitro myogenesis of human embryonic stem cells and their in vivo engraftment. PLoS One, 8(8), e72023. doi:10.1371/journal.pone.0072023 [PubMed: 23977197]

Jiwlawat S, Lynch E, Glaser J, Smit-Oistad I, Jeffrey J, Van Dyke JM, & Suzuki M (2017). Differentiation and sarcomere formation in skeletal myocytes directly prepared from human induced pluripotent stem cells using a sphere-based culture. Differentiation, 96, 70–81. doi:10.1016/j.diff.2017.07.004 [PubMed: 28915407]

Kusuma S, Smith Q, Facklam A, & Gerecht S (2017). Micropattern size-dependent endothelial differentiation from a human induced pluripotent stem cell line. J Tissue Eng Regen Med, 11(3), 855–861. doi:10.1002/term.1985 [PubMed: 25641688]

Lim JA, Li L, & Raben N (2014). Pompe disease: from pathophysiology to therapy and back again. Front Aging Neurosci, 6, 177. doi:10.3389/fnagi.2014.00177 [PubMed: 25183957]

Ludwig TE, Bergendahl V, Levenstein ME, Yu J, Probasco MD, & Thomson JA (2006). Feeder-independent culture of human embryonic stem cells. Nat Methods, 3(8), 637–646. doi:10.1038/nmeth902 [PubMed: 16862139]

Madden L, Juhas M, Kraus WE, Truskey GA, & Bursac N (2015). Bioengineered human myobundles mimic clinical responses of skeletal muscle to drugs. Elife, 4, e04885. doi:10.7554/eLife.04885 [PubMed: 25575180]

Maffioletti SM, Gerli MF, Ragazzi M, Dastidar S, Benedetti S, Loperfido M, … Tedesco FS. (2015). Efficient derivation and inducible differentiation of expandable skeletal myogenic cells from

human ES and patient-specific iPS cells. Nat Protoc, 10(7), 941–958. doi:10.1038/nprot.2015.057 [PubMed: 26042384]

Maffioletti SM, Sarcar S, Henderson ABH, Mannhardt I, Pinton L, Moyle LA, … Tedesco FS. (2018). Three-Dimensional Human iPSC-Derived Artificial Skeletal Muscles Model Muscular Dystrophies and Enable Multilineage Tissue Engineering. Cell Rep, 23(3), 899–908. doi:10.1016/j.celrep.2018.03.091 [PubMed: 29669293]

Manganelli F, & Ruggiero L (2013). Clinical features of Pompe disease. Acta Myol, 32(2), 82–84. [PubMed: 24399863]

Murrell M, Kamm R, & Matsudaira P (2011). Substrate viscosity enhances correlation in epithelial sheet movement. Biophys J, 101(2), 297–306. doi:10.1016/j.bpj.2011.05.048 [PubMed: 21767481]

Nakamoto T, Wang X, Kawazoe N, & Chen G (2014). Influence of micropattern width on differentiation of human mesenchymal stem cells to vascular smooth muscle cells. Colloids Surf B Biointerfaces, 122, 316–323. doi:10.1016/j.colsurfb.2014.06.013 [PubMed: 25064482]

Palchesko RN, Zhang L, Sun Y, & Feinberg AW (2012). Development of polydimethylsiloxane substrates with tunable elastic modulus to study cell mechanobiology in muscle and nerve. PLoS One, 7(12), e51499. doi:10.1371/journal.pone.0051499 [PubMed: 23240031]

Prater SN, Patel TT, Buckley AF, Mandel H, Vlodavski E, Banugaria SG, … Kishnani PS. (2013). Skeletal muscle pathology of infantile Pompe disease during long-term enzyme replacement therapy. Orphanet J Rare Dis, 8, 90. doi:10.1186/1750-1172-8-90 [PubMed: 23787031]

Rao L, Qian Y, Khodabukus A, Ribar T, & Bursac N (2018). Engineering human pluripotent stem cells into a functional skeletal muscle tissue. Nat Commun, 9(1), 126. doi:10.1038/s41467-017-02636-4 [PubMed: 29317646]

Raval KK, Tao R, White BE, De Lange WJ, Koonce CH, Yu J, … Kamp TJ. (2015). Pompe disease results in a Golgi-based glycosylation deficit in human induced pluripotent stem cell-derived cardiomyocytes. J Biol Chem, 290(5), 3121–3136. doi:10.1074/jbc.M114.628628 [PubMed: 25488666]

Reuser AJ, Koster JF, Hoogeveen A, & Galjaard H (1978). Biochemical, immunological, and cell genetic studies in glycogenosis type II. Am J Hum Genet, 30(2), 132–143. [PubMed: 350041]

Rinaldi F, & Perlingeiro RC (2014). Stem cells for skeletal muscle regeneration: therapeutic potential and roadblocks. Transl Res, 163(4), 409–417. doi:10.1016/j.trsl.2013.11.006 [PubMed: 24299739]

Roca I, Requena J, Edel MJ, & Alvarez-Palomo AB (2015). Myogenic Precursors from iPS Cells for Skeletal Muscle Cell Replacement Therapy. J Clin Med, 4(2), 243–259. doi:10.3390/jcm4020243 [PubMed: 26239126]

Saha K, Keung AJ, Irwin EF, Li Y, Little L, Schaffer DV, & Healy KE (2008). Substrate modulus directs neural stem cell behavior. Biophys J, 95(9), 4426–4438. doi:10.1529/biophysj.108.132217 [PubMed: 18658232]

Sale DM a D. (2014). The Physiology of Training for High Performance: Oxford University Press.

Salick MR, Napiwocki BN, Sha J, Knight GT, Chindhy SA, Kamp TJ, … Crone WC. (2014). Micropattern width dependent sarcomere development in human ESC-derived cardiomyocytes. Biomaterials, 35(15), 4454–4464. doi:10.1016/j.biomaterials.2014.02.001 [PubMed: 24582552]

Serena E, Zatti S, Reghelin E, Pasut A, Cimetta E, & Elvassore N (2010). Soft substrates drive optimal differentiation of human healthy and dystrophic myotubes. Integr Biol (Camb), 2(4), 193–201. doi:10.1039/b921401a [PubMed: 20473399]

Serena E, Zatti S, Zoso A, Lo Verso F, Tedesco FS, Cossu G, & Elvassore N (2016). Skeletal Muscle Differentiation on a Chip Shows Human Donor Mesoangioblasts' Efficiency in Restoring Dystrophin in a Duchenne Muscular Dystrophy Model. Stem Cells Transl Med, 5(12), 1676–1683. doi:10.5966/sctm.2015-0053 [PubMed: 27502519]

Sha J, Lippmann ES, McNulty J, Ma Y, & Ashton RS (2013). Sequential nucleophilic substitutions permit orthogonal click functionalization of multicomponent PEG brushes. Biomacromolecules, 14(9), 3294–3303. doi:10.1021/bm400900r [PubMed: 23937610]

Shelton M, Metz J, Liu J, Carpenedo RL, Demers SP, Stanford WL, & Skerjanc IS (2014). Derivation and expansion of PAX7-positive muscle progenitors from human and mouse embryonic stem cells. Stem Cell Reports, 3(3), 516–529. doi:10.1016/j.stemcr.2014.07.001 [PubMed: 25241748]

Skoglund G, Laine J, Darabi R, Fournier E, Perlingeiro R, & Tabti N (2014). Physiological and ultrastructural features of human induced pluripotent and embryonic stem cell-derived skeletal myocytes in vitro. Proc Natl Acad Sci U S A, 111(22), 8275–8280. doi:10.1073/pnas.1322258111 [PubMed: 24843168]

Takikita S, Myerowitz R, Zaal K, Raben N, & Plotz PH (2009). Murine muscle cell models for Pompe disease and their use in studying therapeutic approaches. Mol Genet Metab, 96(4), 208–217. doi: 10.1016/j.ymgme.2008.12.012 [PubMed: 19167256]

Tanaka A, Woltjen K, Miyake K, Hotta A, Ikeya M, Yamamoto T, … Sakurai H. (2013). Efficient and reproducible myogenic differentiation from human iPS cells: prospects for modeling Miyoshi Myopathy in vitro. PLoS One, 8(4), e61540. doi:10.1371/journal.pone.0061540 [PubMed: 23626698]

Tedesco FS, & Cossu G (2012). Stem cell therapies for muscle disorders. Curr Opin Neurol, 25(5), 597–603. doi:10.1097/WCO.0b013e328357f288 [PubMed: 22918488]

Thurberg BL, Lynch Maloney C, Vaccaro C, Afonso K, Tsai AC, Bossen E, … O'Callaghan M. (2006). Characterization of pre- and post-treatment pathology after enzyme replacement therapy for Pompe disease. Lab Invest, 86(12), 1208–1220. doi:10.1038/labinvest.3700484 [PubMed: 17075580]

Vainzof M, Ayub-Guerrieri D, Onofre PC, Martins PC, Lopes VF, Zilberztajn D, … Yamamoto LU. (2008). Animal models for genetic neuromuscular diseases. J Mol Neurosci, 34(3), 241–248. doi: 10.1007/s12031-007-9023-9 [PubMed: 18202836]

van der Wal E, Bergsma AJ, van Gestel TJM, In 't Groen SLM, Zaehres H, Arauzo-Bravo MJ, … Pijnappel W. (2017). GAA Deficiency in Pompe Disease Is Alleviated by Exon Inclusion in iPSC-Derived Skeletal Muscle Cells. Mol Ther Nucleic Acids, 7, 101–115. doi:10.1016/j.omtn. 2017.03.002 [PubMed: 28624186]

Wang X, Song W, Kawazoe N, & Chen G (2013). The osteogenic differentiation of mesenchymal stem cells by controlled cell-cell interaction on micropatterned surfaces. J Biomed Mater Res A, 101(12), 3388–3395. doi:10.1002/jbm.a.34645 [PubMed: 23554043]

Werneck LC, Lorenzoni PJ, Kay CS, & Scola RH (2013). Muscle biopsy in Pompe disease. Arq Neuropsiquiatr, 71(5), 284–289. [PubMed: 23689405]

Xu C, Tabebordbar M, Iovino S, Ciarlo C, Liu J, Castiglioni A, … Zon LI. (2013). A zebrafish embryo culture system defines factors that promote vertebrate myogenesis across species. Cell, 155(4), 909–921. doi:10.1016/j.cell.2013.10.023 [PubMed: 24209627]

Yaffe D, & Feldman M (1965). The Formation of Hybrid Multinucleated Muscle Fibers from Myoblasts of Different Genetic Origin. Dev Biol, 11, 300–317. [PubMed: 14332576]

Yanagisawa M, Mukai A, Shiomi K, Song SY, & Hashimoto N (2011). Community effect triggers terminal differentiation of myogenic cells derived from muscle satellite cells by quenching Smad signaling. Exp Cell Res, 317(2), 221–233. doi:10.1016/j.yexcr.2010.10.011 [PubMed: 20965167]

Yoshida T, Awaya T, Jonouchi T, Kimura R, Kimura S, Era T, … Sakurai H. (2017). A Skeletal Muscle Model of Infantile-onset Pompe Disease with Patient-specific iPS Cells. Sci Rep, 7(1), 13473. doi: 10.1038/s41598-017-14063-y [PubMed: 29044175]

Yu H, Xiong S, Tay CY, Leong WS, & Tan LP (2012). A novel and simple microcontact printing technique for tacky, soft substrates and/or complex surfaces in soft tissue engineering. Acta Biomater, 8(3), 1267–1272. doi:10.1016/j.actbio.2011.09.006 [PubMed: 21945825]

Yu J, Hu K, Smuga-Otto K, Tian S, Stewart R, Slukvin II, & Thomson JA (2009). Human induced pluripotent stem cells free of vector and transgene sequences. Science, 324(5928), 797–801. doi: 10.1126/science.1172482 [PubMed: 19325077]

Yu J, Vodyanik MA, Smuga-Otto K, Antosiewicz-Bourget J, Frane JL, Tian S, … Thomson JA. (2007). Induced pluripotent stem cell lines derived from human somatic cells. Science, 318(5858), 1917–1920. doi:10.1126/science.1151526 [PubMed: 18029452]

Zatti S, Zoso A, Serena E, Luni C, Cimetta E, & Elvassore N (2012). Micropatterning topology on soft substrates affects myoblast proliferation and differentiation. Langmuir, 28(5), 2718–2726. doi: 10.1021/la204776e [PubMed: 22217143]

Zhu X, Fu L, Yi F, Liu GH, Ocampo A, Qu J, & Izpisua Belmonte JC (2014). Regeneration: making muscle from hPSCs. Cell Res, 24(10), 1159–1161. doi:10.1038/cr.2014.91 [PubMed: 25001388]

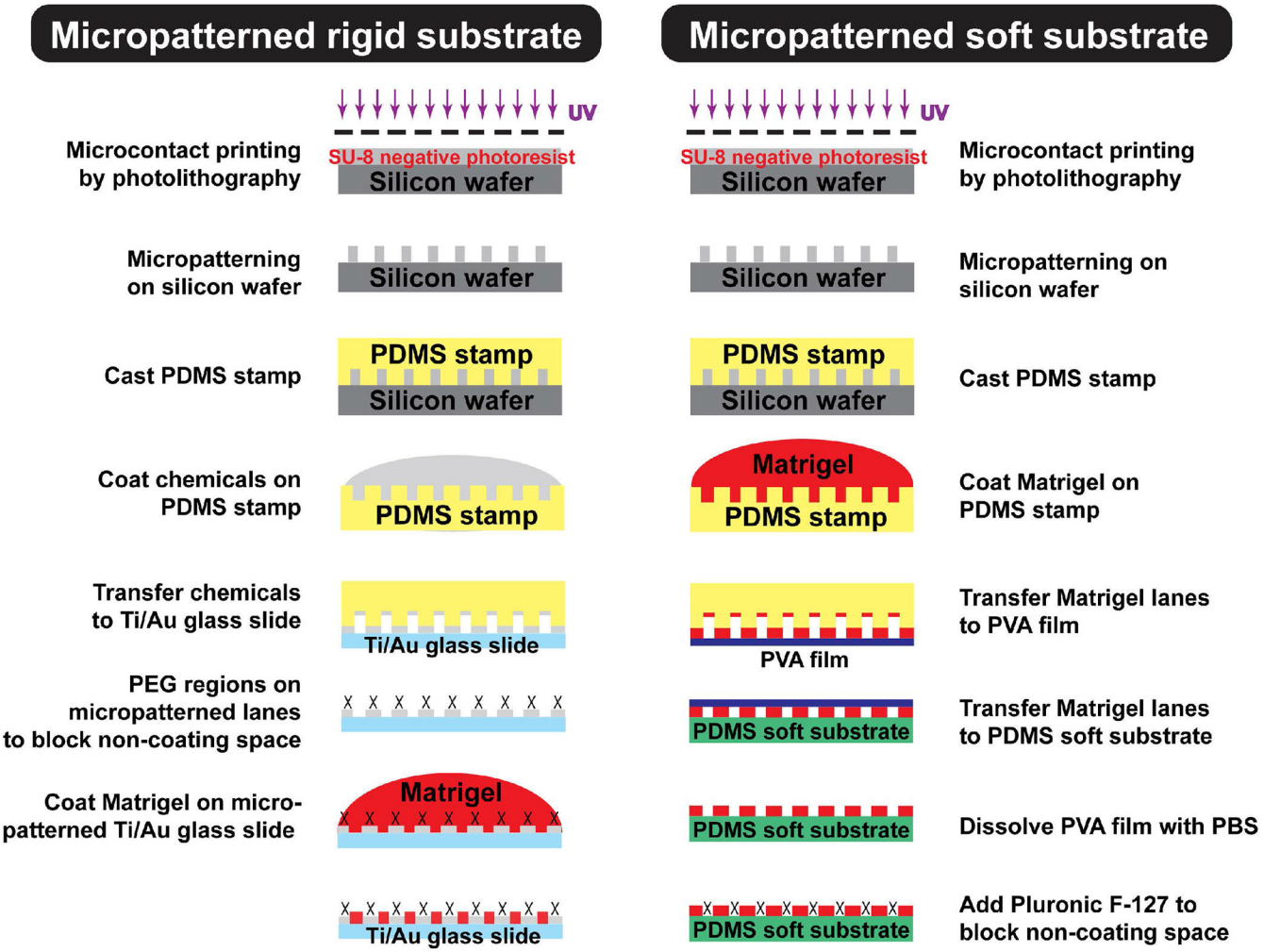

Figure 1. Preparation of micropatterned culture platforms with varying stiffnesses.

Micropatterned rigid substrate (Left) and micropatterned soft substrate (Right). Photolithography was used to create micropatterns on the silicon wafer and polydimethylsiloxane (PDMS) was poured on the silicon wafer to make PDMS stamps. For micropatterning on rigid substrates, chemicals (ω-mercaptoundecyl bromoi-sobutyrate) were coated on the PDMS stamp and then transferred to Ti/Au-glass slide to generate non-adherent polyethylene glycol (PEG) regions, which prevented cell attachment to non-Matrigel areas. For micropatterning on soft substrates, PDMS stamps coated with Matrigel were first transferred to a polyvinyl alcohol (PVA) film. The PVA film containing Matrigel lanes was then placed on the 15kPa PDMS soft substrate. PVA films were dissolved with PBS and Pluronic F-127 was added to the substrate to prevent cell attachment in the non-Matrigel areas.

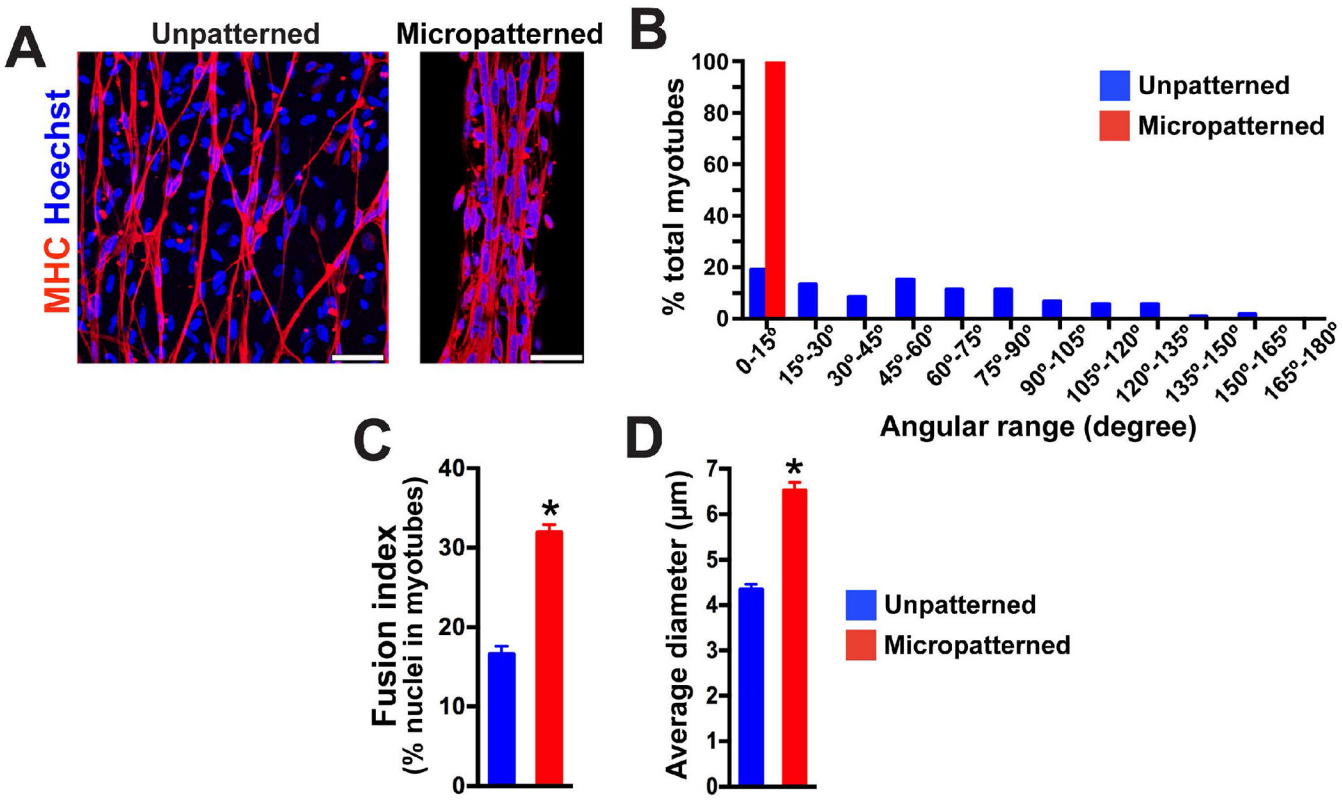

Figure 2. Micropatterning on rigid substrate enhances alignment and fusion of iPSC-derived myotubes.

(A) Representative images of immunocytochemistry labeled myosin heavy chain (MHC) after 2 weeks of terminal differentiation on a patterned or unpatterned rigid substrate. Multiple nuclei were lined up and fused in MHC^+ myotubes on micropatterned lanes. In contrast, single fusion was identified for cells cultured on unpatterned geometry. Scale bar = 50 μm. **(B)** The myotubes on micropatterned lanes (n = 100) were highly-aligned within a 15° angle of lane direction compared to the myotubes on an unpatterned platform (n = 116). **(C)** Fusion index analysis revealed that more nuclei were fused together in MHC^+ myotubes on micropatterned lanes compared to the myotubes on unpatterned platforms. Fifteen and sixteen microscopic fields from micropatterned and unpatterned culture were used for analysis respectively. **(D)** Micropatterned geometry increased myotube diameter. (n = 100 in micropatterned, n = 116 in unpatterned; *p< 0.01)

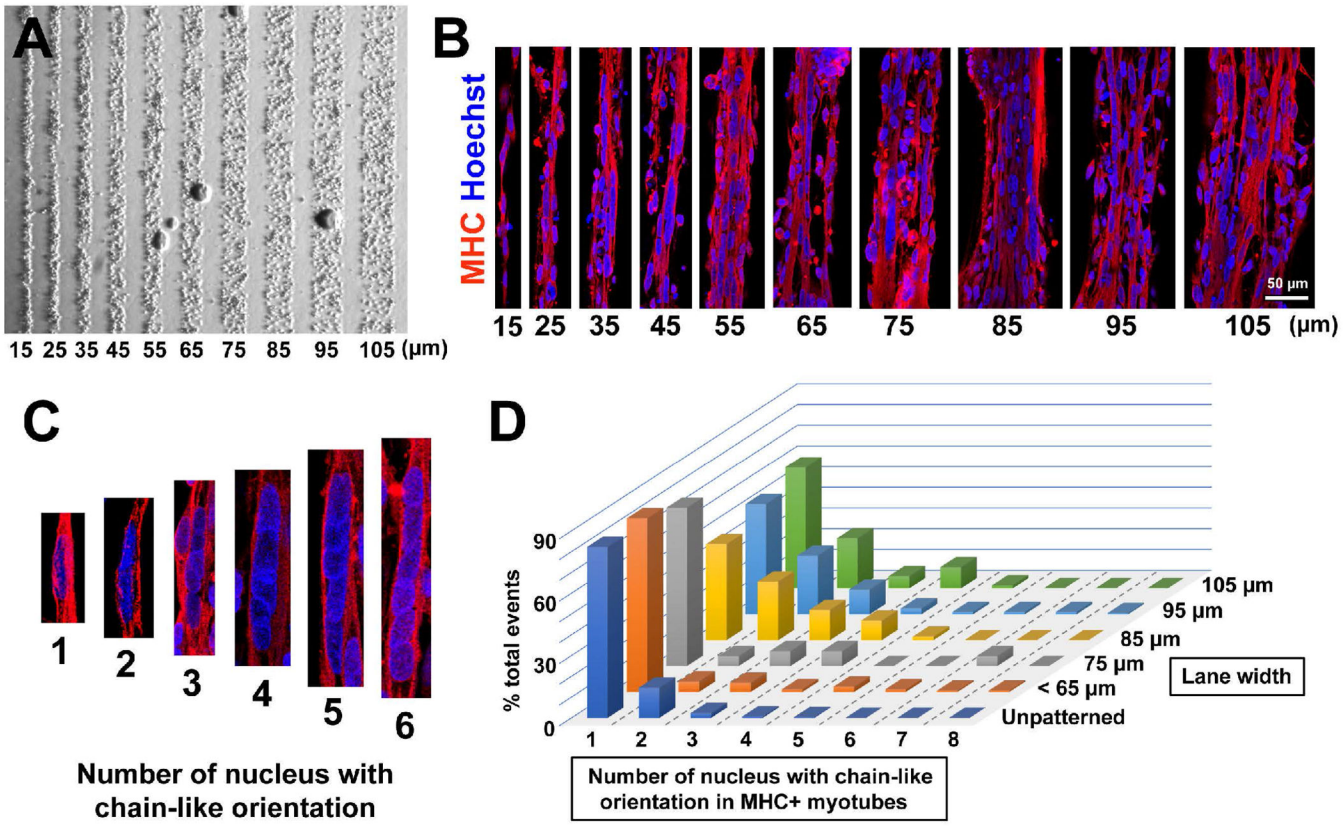

Figure 3. Micropatterned lane width on rigid substrate influences fusion of control iPSC-derived myotubes.

(A) Representative bright field images of control line iPSC-myogenic progenitors after a few hours of plating on rigid substrate micropatterned lanes. The cells attached on Matrigel-coated lanes and were restricted by PEG regions. **(B)** At 2 weeks of differentiation, MHC^{+} myotubes were linearly aligned on the micropatterned lanes with specific widths between 15 and 105 μm. Scale bar = 50 μm. **(C)** Representative images of aligned cell nuceli in the differentiated myotubes. **(D)** A lane width of 85 μm produced the highest occurrence of multiple (2-4) nuclear fusion in a chain-like orientation, and was therefore used for the remainder of the study.

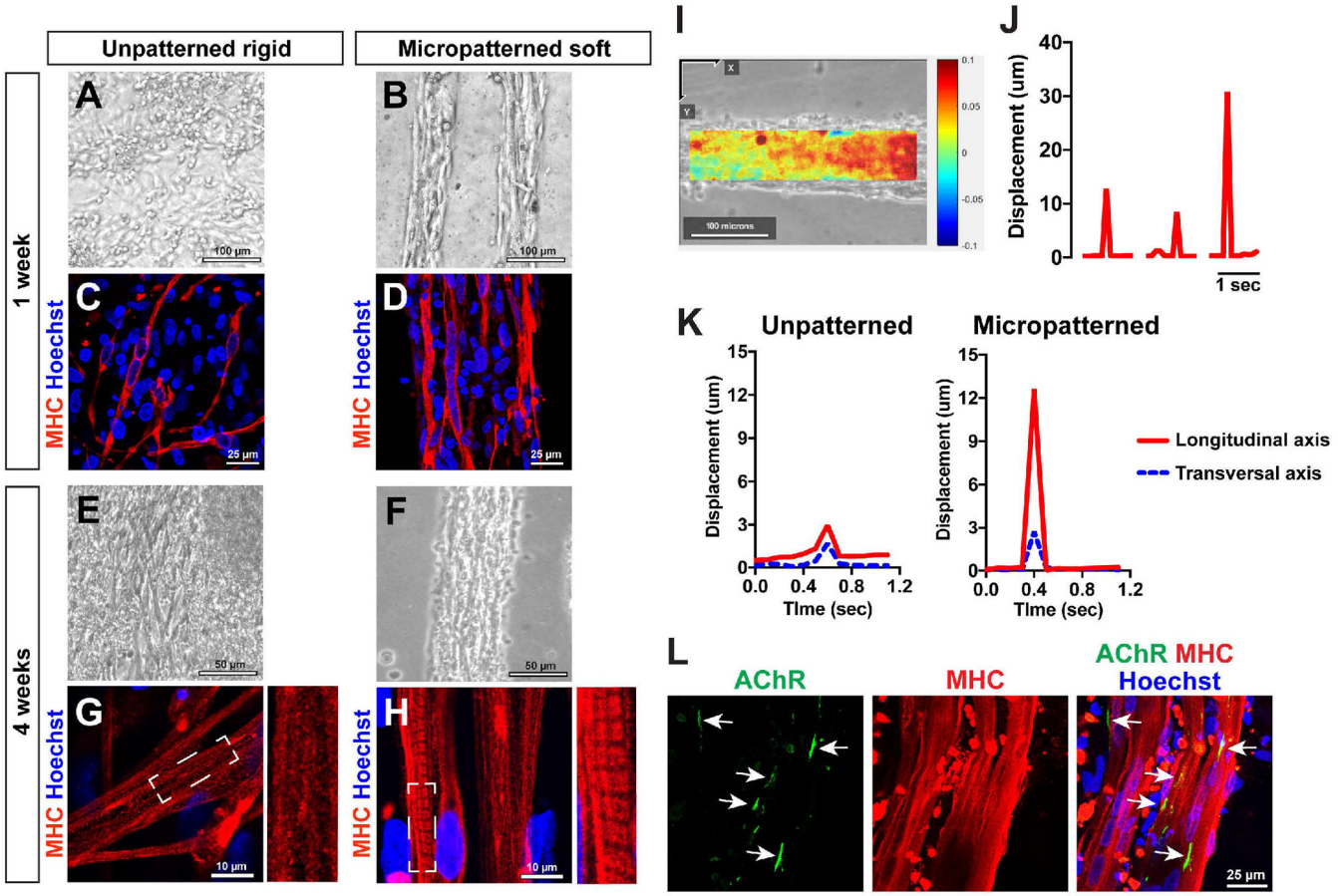

Figure 4. Micropatterned soft substrates enhance sarcomere formation, differentiation, and maturation of control iPSC-derived myotubes.

Representative bright field images of plated myotubes; myotubes on unpatterned substrates were irregularly distributed at 1 week **(A)** and 4 weeks **(E)** of differentiation. In contrast, highly-aligned myotubes were maintained on micropatterned lanes with controlled stiffness **(B and F)**. MHC immunocytochemistry revealed that micropatterned soft substrates induced more multi-nuclear fusion in iPSC-derived myotubes **(D)** than the unpatterned culture **(C)**. Represented by striated patterns of MHC-positive signals, sarcomere structures were visible in the myotubes on micropatterned soft substrates at 4 weeks of differentiation **(H)**, although such subcellular characteristic was not identified in the myotubes plating on unpatterned rigid substrates **(G)**. **(I)** Representative image field analyzed by digital image correlation (DIC) in the myotube contraction videos. The heatmap is created using contracted and at rest video frames, with positive displacement (red) in the longitudinal (X-axis) direction. **(J)** The displacement change quantifies individual contractions. Representative changes of maximum displacement from the entire field of view are plotted for three contraction events. **(K)** The displacements in the transverse and longitudinal direction during the course of a single contraction. The unpatterned myotubes had similar displacements in two directions, while the myotubes plated on micropatterned lanes had a much larger displacement longitudinally along the lane axis, with minimal displacement in the transverse direction. **(L)**

Immunostaining against alpha-bungarotoxin was used to label acetylcholine receptors (AChR) (arrows) on MHC^+ myotubes.

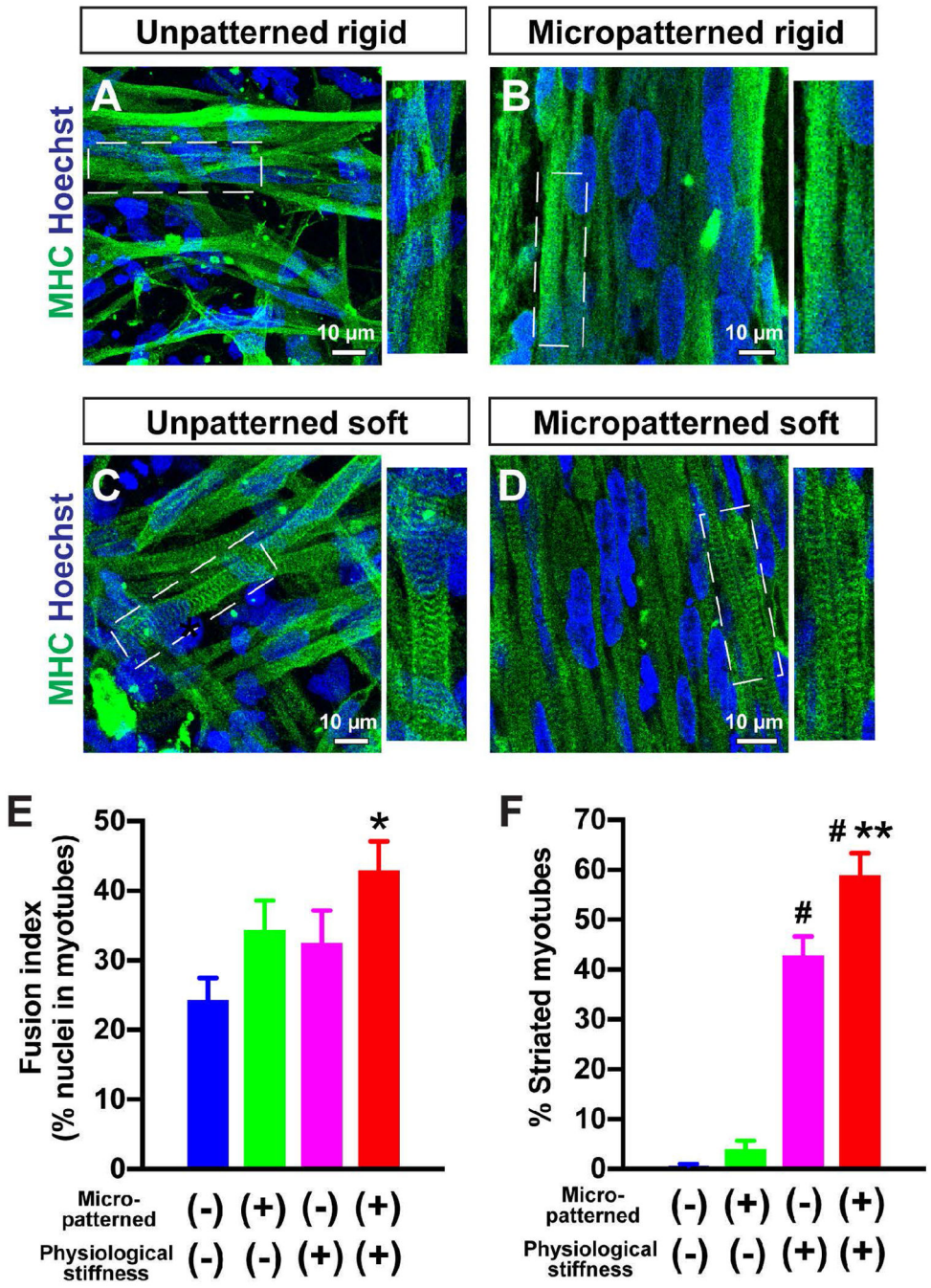

Figure 5. Micropatterning and physiological surface stiffness further promote myotube striation in control iPSC-derived myotubes.

Immunofluorescence staining of MHC and Hoechst of healthy control iPSC-derived myotubes at 2 weeks of differentiation **(A-D)**. The micropatterned feature resulted in linear alignment of MHC^{+} myotubes **(B, D)**. Whereas myotube striation was remarkably formed on the soft substrates with either unpatterned **(C)** or micropatterned **(D)** geometries, myotubes on the rigid substrate did not show obvious striation at 2 weeks of differentiation **(A, B)** The percentage of striated myotubes was significantly higher on micropatterned (n =

16 fields) and unpatterned (n = 16 fields) soft substrates, compared with unpatterned rigid substrate (n = 10 fields). *p< 0.05 vs. Unpatterned rigid in **E**. #p< 0.05 vs. Unpatterned soft and micropatterned rigid, and **p< 0.05 vs. Unpatterned soft in **F**.

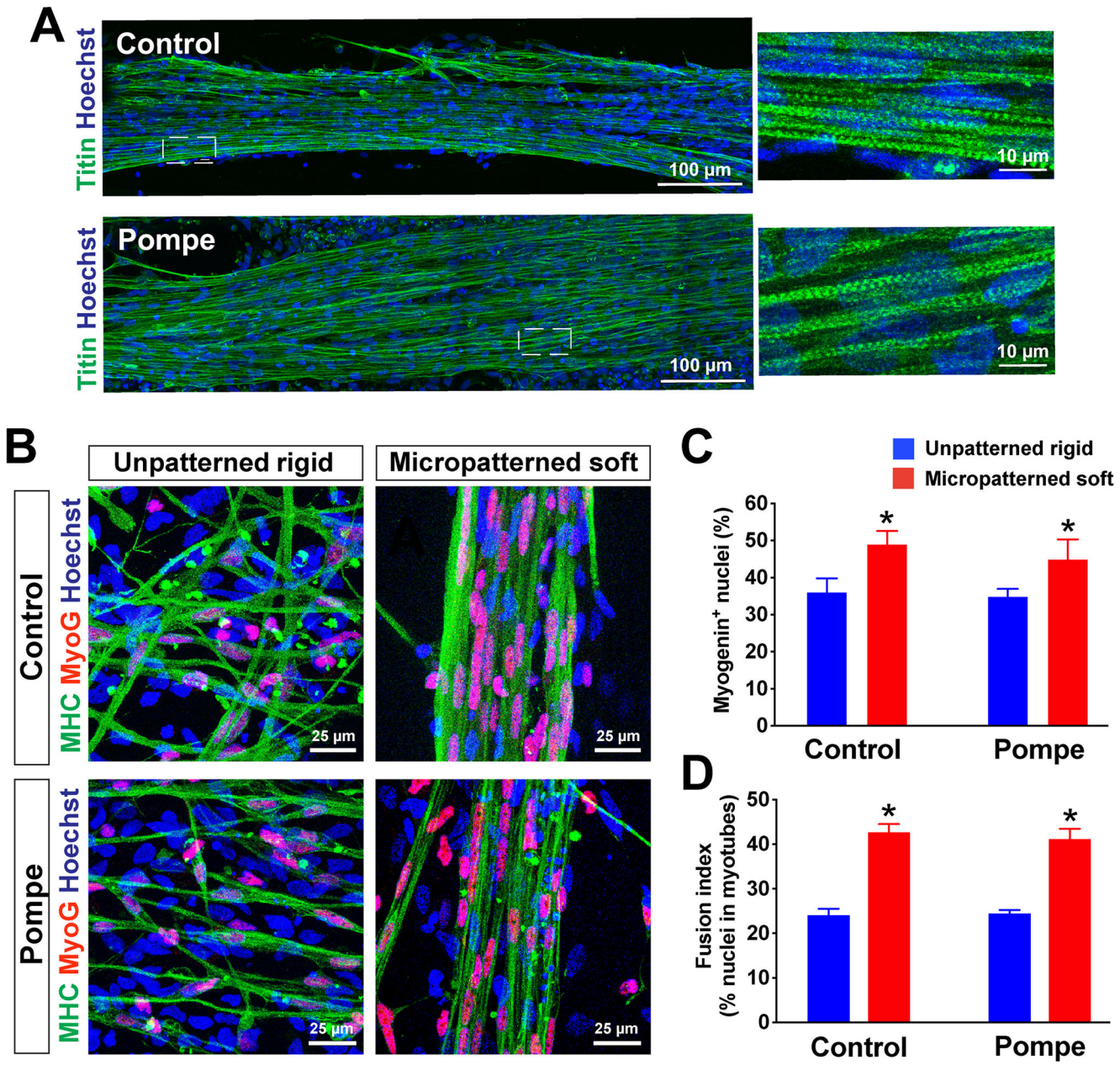

Figure 6. Differentiation of patient iPSC-derived myotubes with Pompe disease using micropatterned substrates.

(A) Immunostaining of elastic myofilaments (titin) on control- and Pompe-iPSC derived myotubes. Titin+ myotubes, which had a length of over 750 μm were positively labeled on a micropatterned soft substrate derived from both control and Pompe iPSCs at 2 weeks of differentiation. **(B)** Immnostaining of myogenin (MyoG) and MHC in healthy (control) and Pompe iPSC-derived myotubes. Almost all of the nuclei in MHC^{+} myotubes were positive with myogenin, which represent committed myocytes. The micropatterned feature increased multi-nuclear fusions, while each myotube on unpatterned feature had only one nucleus or a single fusion with two nuclei. The number of MyoG+ nuclei **(C)** and fusion index **(D)**

increased when plated on micropatterned lanes (n = 6 fields) than on unpatterned platforms (n = 6 fields). *p< 0.05 vs. Unpatterned rigid.

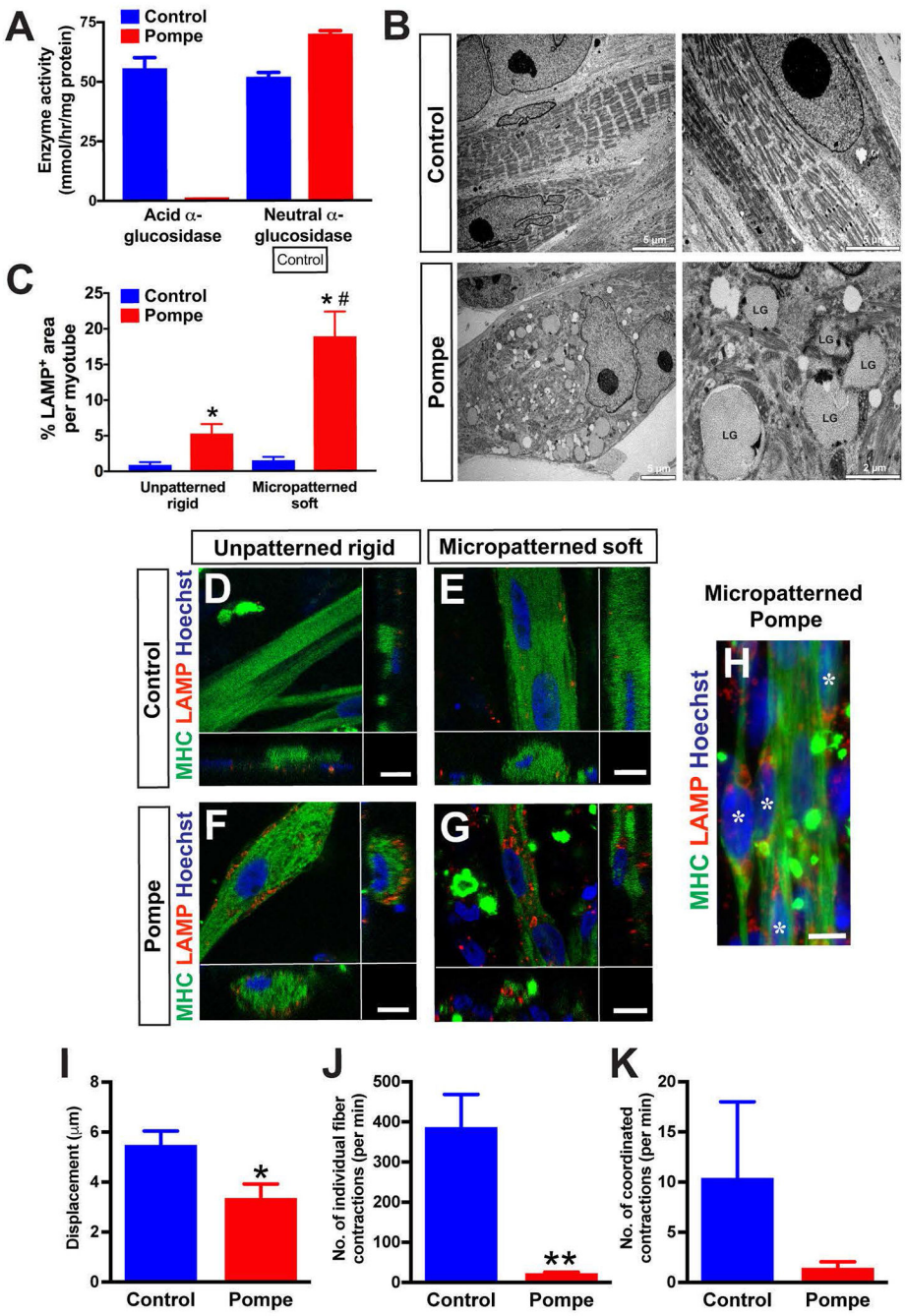

Figure 7. Pompe iPSC-derived myotubes exhibited specific disease phenotypes.

(A) Pompe iPSC-derived myogenic progenitors have no acid alpha-glucosidase enzyme activity, while a significant level of neutral α-glucosidase (control) was detectable in the same cell lines. n = 3 from three individual experiments. *p< 0.05 vs. control cells. **(B)** Ultrastructure of Pompe iPSC-derived myotubes. Whereas the myofibrils derived from control iPSCs had well-organized sarcomere structure, Pompe iPSC-derived myotubes contained multiple enlarged lysosomes with glycogen accumulation. LG: Lysosomal glycogen. **(C)** The percentage of the LAMP-positive area per myotube. *p< 0.01 vs.

Control; #p< 0.01 vs. Unpatterned Pompe. Compared to the myotubes derived from healthy control iPSCs **(D and E)**, Pompe iPSC-derived myotubes had increased LAMP1+ signals at 6 weeks of differentiation **(F, G, H)**. In **H**, LAMP-positive myotubes (asterisks) are in bundle-like structures when cultured in micropatterned lanes. Scale bar = 10 μm. **(I)** DIC analysis showed a decrease of the maximum displacement averaged from several contraction events. *p< 0.05 vs. control cells. **(J)** Pompe iPSC-derived myotubes had significantly less total contractions per minute compared to control myotubes. **p< 0.01 vs. control cells. **(K)** Simiarly, the average number of coordinated full-bundle contractions per minute tended to be less in Pompe disease myotubes, although the difference did not reach significance.